COMPOSITE NANOCLAY-HYDROXYAPATITE-POLYMER FIBER SCAFFOLDS FOR BONE TISSUE ENGINEERING USING PRESSURE GYRATION

Krishna Kundu[1], Ayda Afshar[2], Dinesh Katti[1], Mohan Edirisinghe[2], Kalpana Katti[1*]

[1] Center for Engineered Cancer Testbeds, Department of Civil and Environmental Engineering, North Dakota State University, Fargo, ND 58108, USA.

[2] Department of Mechanical Engineering, University College London, London WC1E 7JE, UK.

* Corresponding author: kalpana.katti@ndsu.edu

ABSTRACT

A novel fabrication of polymer composite fibers using polycaprolactone (PCL), montmorillonite nanoclay (MMT-Clay), and nano-hydroxyapatite-clay (HAP MMT-Clay) is reported for bone tissue engineering applications. Using a pressurized gyration (PG) setup, polycaprolactone (PCL) fibers incorporated with *in situ* mineralized HAP MMT-Clay and MMT-Clay were investigated. Using the novel fabrication method, we were able to successfully manufacture HAP-nanoclay-PCL fibers. Further, 3D scaffolds made using the prepared fibers were able to enhance bone growth, cell viability, and proliferation. The results demonstrated that the polymer fiber scaffolds are biocompatible, and the cells were able to thrive and differentiate on the fiber scaffolds. A significant increase in cell viability, osteogenic differentiation, ECM formation, and collagen formation was observed with PCL HAP MMT-Clay fibers scaffolds compared to the behaviors in PCL fibers. Further, the intracellular ALP levels increased with PCL HAP MMT-Clay fiber scaffold, indicating enhanced osteogenic differentiation of MSCs. This work shows a promising outlook for the future of manufacturable composite nanoclay polymer fibers incorporated as scaffolds for bone tissue engineering applications.

Keywords: biomaterial composites; fiber; biomaterials; bone; scaffolds; pressurized gyration

1. INTRODUCTION

While numerous operational techniques such as bone autografts, allografts, and biomaterials implantation with biocompatible, osteointegrative, and osteoconductive properties are available, they have significant limitations[1]. Post-surgery, autografts are often accompanied by nerve damage, infections, morbidity, scarring, and chronic pain[2–4]. Additionally, allografts can potentially cause disease conductivity, infection and incite immune reactions following the implant rejection. Researchers have attempted to overcome these complications using natural or synthetic biomaterials. Moreover, the alternative to traditional bone grafting therapies is using an engineered scaffold designed to support cell migration, regeneration, and proliferation[5–7]. Cellular growth and attachment are largely dependent on both the pores' size and density within a scaffold, which, depending on the materials and applications, must be carefully controlled to specific parameters. One of the main reasons why porosity is important is that cellular networks rely on interconnected pathways for nutrient transportation and cell proliferation, imitating the structure of the native extracellular matrix (ECM) environment[8–12]. Scaffolds are intended to serve as fillers that occupy bone defects or available space in damaged organs/ tissues. Their resorption activity enables them to provide a basis for new tissue growth that will replace the scaffolds[13–15]. A multifunctional scaffold must be produced to modulate the balance between bone resorption and bone regeneration to repair bone defects[16]. The demand for developing new bioactive scaffolds is growing, promoting the formation of functional tissues by directing stem cell differentiation. Often critical-sized-bone-defects or defects that lack the ability to heal spontaneously without medical intervention are at least two times the diameter of the bone[17]. Such defects require filling with scaffold systems that are also able to bear load[18]. Putty-type materials are required for filling around the larger scaffolds. The

nanocomposite fiber materials presented here are good candidates for use as packing cement around scaffolds for large and critical-sized defects and are novel candidates for filling smaller bone defects.

Polymeric fibers have been extensively used to prepare porous polymer scaffolds for tissue engineering applications in the form of woven and nonwoven fibers[19,20], often for non-union and non-load-bearing applications. There are several techniques to prepare nanofibers, such as phase separation[21], template synthesis[22], self-assembly[23], and electrospinning[24,25]. Usually, spinning techniques are used to prepare nonwoven polymer fibers using polymer solutions or melt[26,27]. The spinning technique can produce the fibers in the nano- to micrometer range, resembles the collagen fibers in the extracellular matrix (ECM)[28–30]. These fibers have a high surface-area-to-volume ratio, a low density, and a high surface volume[31]. Among these techniques, electrospinning is the most popular technique. Still, it has several drawbacks, such as a low production rate, utilization of very high voltage, and sensitivity to the polymer solution's dielectric constant. Those drawbacks demand a novel, cost-effective technique to fabricate nanofibers with a high production rate[32]. Typically, pressurized gyration generates fibers with the combination of centrifugal and dynamic fluid flow forces, which act against surface tension. As the pressurized gyration consists of simultaneous centrifugal spinning and solution blowing, fibers size, diameter, morphology is greatly influenced by the rotation speed and pressure of the process[32,33]. Polymer concentration and the evaporation rate of the solvent determine the yield and the quality of the fibers. This technique has been widely used to prepare nanofibers from various polymers for different applications, such as drug delivery and tissue engineering[32–35].

Some of the most striking characteristics of nanofibers are their high surface to volume ratio and high porosity, which makes it a robust and desirable candidate for bone tissue regeneration[36–

38]. With remarkable interconnectivity between fiber pores, they can form highly porous mesh networks, making them an attractive option for a host of advanced healthcare applications[39–42]. Many therapeutic agents can be individually or simultaneously incorporated with fibers for bone tissue regeneration. Clay/copolymer nanocomposite films are commonly used in bone regeneration applications because they provide mechanical support, and the aspect ratio, the degree of intercalation/exfoliation, and the ionic strength of the clay can be adjusted according to the drug properties before the addition of the clay to the copolymer matrices. To some extent, their morphology replicates that of the native extracellular matrix (ECM), which is prolific to faster tissue regeneration[43,44]. In general, if the physical interaction between the drug and the fibrous scaffold is optimized to tailor the average pore size of the target drug, higher drug loading efficiency can be achieved. To achieve a preferred fiber diameter for drug delivery applications, it is important to optimize the spinning parameters.

Among various polymers, PCL is a semi-crystalline and hydrophobic polymer that has gained attention in musculoskeletal tissue engineering because of its biocompatibility and superior mechanical properties[45]. It can be used to produce a wide range of scaffolding materials[46]. However, some of the problems associated with PCL include its slow *in vivo* degradation rate and lack of bioactive characteristics[47]. The degradation properties of PCL can be enhanced by integrating nanoparticles such as hydroxyapatite, silica, magnetic nanoparticles, and clays into polymer scaffolds[48–50] or by combining PCL with other rapidly degrading polymers.

In cell-based regeneration therapy, cell-scaffold interaction is very important for the new tissue formations, as cells require a three-dimensional environment with proper stimuli to form tissue. After introducing cell-based regeneration therapy in the early 1990s[51], numerous works have been done to optimize the scaffold's various properties to provide the appropriate environment

for the cells with adequate biophysical and biochemical stimuli to accelerate the regeneration process. One of the significant challenges in the field of tissue engineering is to incorporate these properties into the scaffold. Different inorganic fillers are added to the scaffold to improve cell adhesion, cell-scaffold interaction and facilitate tissue formation for tissue engineering purposes. Hydroxyapatite (HAP) nano-clay has a strong resemblance to the mineral bone; it provides adequate calcification sites while increasing biocompatibility and osteoconductivity of the scaffold[52–55]. Synthetic HAP can form a chemical bond with the host tissue and offers a greater benefit in clinical applications than most other bone substitutes such as allografts or metallic implants. HAP has been reported to enhance osteoblast cell attachment and proliferation, which is a highly desired characteristic for bone defect fillers and to promote bone growth when placed in differentiated bone cells[56–58]. The addition of HAP to polymeric fibers is crucial for bone tissue engineering. Synthetic HAP has excellent osteoconductive and osteoinductive abilities and exhibits slow biodegradability and biocompatibility[59]. The biocompatibility with soft tissue such as skin and muscles makes it ideal for bone regeneration, bone augmentation, bone-implant coating, and dental implants[18].

Other trace elements, such as sodium, magnesium, and silicon, are also used in the scaffold with HAP to improve bioactivity, cell attachment, cell differentiation, bone formation, and mineralization[60–63]. Sodium montmorillonite (Na-MMT) clay is the most commonly used layered silicate for the preparation of polymer-clay nanocomposites for its high surface-to-volume ratio and high aspect ratio at low filler content (> 5%), which helps to establish better interaction with the polymer matrix and to enhance the mechanical properties[64–66]. The nanometer thickness of the MMT layer provides a high aspect ratio that can also help obtain a cellular response that favors tissue formation as nanoscale features facilitate cell adhesion and increase the biodegradability of the scaffolds [66–68].

Mesenchymal stem cells (MSCs) have been considered as the cell source for tissue-engineering applications due to their ease of isolation, ability to proliferate in an undifferentiated state[69], capability of differentiating into different cell lineages including bone[70,71], ligament[72], adipose[73], cartilage[74,75], and muscle[76]. MSCs have been seeded on the porous scaffold and implanted on the animal model to repair bone defects [77,78] directly in several studies. The co-culture of osteoblast cells with MSCs induce the osteogenic differentiation of MSCs[18]. Osteoblast cells enhance the osteogenic differentiation by a direct cell-to-cell interaction[79,80] and are critically involved in bone remodeling[81].

In this study, we investigate the feasibility of fiber-based nanoclay scaffolds for bone tissue engineering applications. We observed the effect of HAP-Clay in polymeric fibers scaffold in terms of cell viability, cell proliferation, osteogenesis, mineral depositions, and collagen fiber formations, which are the essential elements of bone regeneration.

2. MATERIALS AND METHODS

2.1 Materials for fibers

2.1.1 Modification of MMT clay

The detailed procedure for the modification of Na-MMT clay is described elsewhere[82–85]. Briefly, 5-aminovaleric acid solution was added to preheated (60^{o}C) MMT suspension, and the mixture solution was kept for stirring. After one hour, the obtained slurry was centrifuged and washed to remove chloride ions followed by drying at 70^{o}C, grinding, and sieving to obtain a fine powder. Na-MMT clay (SWy-2) was procured from Clay Minerals Society. The 5-aminovaleric acid was obtained from Sigma-Aldrich.

2.1.2 Preparation of in situ HAP clay

We have followed the procedure described in previous studies [82–85] to prepare *in situ* HAP clay. Briefly, the organically modified MMT clay powder was dissolved into Na_2HPO_4 solution by stirring at room temperature (25 °C) for 2 hours. Further, the $CaCl_2$ solution was added, and this suspension was stirred vigorously for 8 hours (pH 7.4). The precipitate obtained settled in 12 hours, was centrifuged and dried (70°C). Subsequently, it was ground and sieved to obtain a fine powder. The compounds Na_2HPO_4 and $CaCl_2$ were purchased from J.T. Baker.

2.1.3 Preparation of Polymer and Clay Solution

Polycaprolactone (PCL, M_w 800 00 g mol^{-1}) was purchased from Sigma-Aldrich (Poole, UK). Multiple polycaprolactone (PCL) solutions were prepared at different concentrations. As a result of preliminary testing, it was found that 15 w/v% PCL in chloroform produced the optimal fiber yield. Therefore, 15 w/v% PCL in chloroform was prepared and served as a control sample. Different HAP MMT-Clay and MMT-Clays concentrations (2 w/w % and 5 w/w %) were loaded into PCL polymer solution followed by stirring for 24 h using magnetic stirrers to obtain a homogeneous solution.

2.1.4 Pressurized gyration

Pressurized gyration is a simple technique for mass production of fibers and fibrous structures with controllable fiber size and fiber size distribution with high yield. The setup consists of an aluminum cylindrical vessel (60 mm diameter, 35 mm height) with a total of 24 orifices on the wall of the vessel. Each orifice is 0.5 mm in diameter. The vessel top is connected to a DC motor that generates a maximum speed of 36 000 rpm, and the bottom is connected to a constant nitrogen gas stream (N_2) that generates pressure between 0.1 – 0.3 MPa. The fibers produced by this technique depend on the rotational speed of the vessel, air pressure, and the concentration of the polymer solution. The polymer solution is placed into the vessel before spinning. High speed and high-pressure cause fibers to erupt, elongate, and thin. As the fibers thin, the solvent evaporates from the fiber

strand. In this study, we report the creation of PCL fibers incorporated with HAP MMT nanoclays. The maximum rotation speed was used as it increases the centrifugal force, and as such, the fibers leave at greater kinetic energy and thinness. When increasing pressure, in general, fibers are manufactured thinner due to the gas pressure providing a greater elongation power. However, increased pressure (gas flow) can also increase evaporation, leading to thicker fibers due to increased polymer concentration and higher solution viscosity.

2.1.5 Preparation of fiber scaffold

The polymer composite fibers samples from the pressurized gyration method were received from Edirisinghe-lab, Mechanical Engineering, UCL. A 3D cylindrical scaffold of dimension 3 mm (height) X 10 mm (diameter) was prepared by pressing 0.065g of fibers (Scheme 1), and subsequently, these were used them for cell culture experiments.

Scheme 1. Schematic diagram illustrating the pressurized gyration set up and 3 key phases and 3D scaffold preparation from polymer composite fibers generated by pressurized gyration.

2.2 Cell culture experiments

3D scaffold samples were kept in UV for 45 mins for sterilization. After that, the sample was immersed in 100 % ethanol for 24 h. Then, samples were washed with PBS and kept in the cell culture media for 24 hours before using them for cell culture experiments. Initially, 5 X 10^4 osteoblast cells and 5 X 10^4 MSCs were seeded on each scaffold.

2.2.1 Cell line and culture medium

The human osteoblast cell line (hFOB 1.19) was obtained from ATCC and maintained in a media consist of 90% HyQ Dulbecco's Modified Eagle medium DMEM-12(1:1) from Hyclone, 10% FBS from ATCC, and 0.6% G418 solution (antibiotic) from JR scientific. Human bone marrow Mesenchymal stem cells (MSCs) were obtained from Lonza and maintained in MSCGM™ Bulletkit™ medium. The Bulletkit™ medium was prepared by adding MSCGM™ SingleQuots™ (Lonza) to MSCBM™ (Lonza). All the cells were maintained at 37^{o}C and 5% CO2 in a completely humidified incubator.

2.3 Fiber characterization

2.3.1 Surface morphology of fibers

The surface morphology of the nanoclays containing PCL fibers was studied using scanning electron microscopy (SEM) using a Hitachi HN004, which operated at an accelerating voltage of 5kV. Before analysis, samples were pre-coated with gold sputter using Quorum Q1500R ES for 90 seconds. For diameter, an average of 100 fiber strand readings was measured at random using ImageJ software. The average fiber diameter was created and plotted on histograms using OriginPro (Origin Lab Corporation, Northampton, MA, USA).

2.3.2 WST-1 assay

WST-1 assay was performed in scaffolds seeded with MSCs and human osteoblast cells (1:1). WST-1 (Roche, IN) assay was used to perform cell viability as per the manufacturer's protocol. Briefly, cells were cultured on scaffolds for 7, 14, and 21 days. Following this, cell-seeded scaffolds were removed from the culture medium, washed with PBS, and then placed in a new 48-well plate with a solution comprising 450 ml of DMEM and 50 ml of WST-1 reagent per well before incubating for 4 h in standard humidified condition. After 4 h, scaffolds were removed from the 48-well plates. The

intensity of yellow color, which directly represents the number of live cells (slightly red-colored solution turns yellow as metabolically active cells cleave the tetrazolium salts of WST-1 reagent to formazan), was read at 450 nm using a microplate spectrophotometer (Bio-Rad, Benchmark Plus).

2.3.3 Alkaline phosphate assay

3D fiber scaffolds seeded with MSCs and human osteoblast cells (1:1) were incubated at 37^{o}C, 5% CO_2 under humidified conditions for 7, 14, 21 days. These samples were washed with PBS after incubation, transferred to unused wells of 48-well plates, and 850mL Triton X-100 (1 v/v %solution) was added to each well containing the samples. Cell lysates (250mL) obtained after subjecting the immersed samples to two freeze-thaw cycles (27^{0}C to 37^{0}C) were transferred to new 48-well plates and incubated with p-nitrophenyl phosphate (250mL) at room temperature for 60 min. 3N NaOH (70mL) was further added to the wells, and absorbance readings will be taken at 405 nm using a microplate spectrophotometer (Bio-Rad, Benchmark Plus).

2.3.4 Alizarin red S staining

3D fiber scaffolds seeded with MSCs and human osteoblast cells were incubated at 37^{o}C, 5% CO_2 under humidified conditions for 7, 14 and 21 days and were then washed with PBS before fixing with 4% paraformaldehyde for 15 min. PBS was used to wash the fixed samples. Further 2% Alizarin Red S (ARS) staining solution of 50 µL was dropped on the washed scaffold and kept for 150 s. After 150 s, the scaffold was washed using PBS many times to remove the unbound stain and dried at room temperature for imaging. Images were captured using an inverted microscope at 20× magnification. For quantification, stained samples were immersed into 700 µL of 10% acetic acid solution and incubated at room temperature for 5 min to solubilize the stain, and absorbance of the released Alizarin Red S stain was measured at 405 nm.

2.3.5 Immunocytochemistry assay

3D fiber scaffolds seeded with MSCs and human osteoblast cells were incubated at 37°C, 5% CO_2 under humidified conditions for 21 days. Cell-seeded scaffolds were washed in PBS and fixed in 4% paraformaldehyde (PFA) for 30 min, followed by permeabilizing with 0.2% TritonX-100 in PBS for 5 min. Further, the samples were blocked with 0.2% fish skin gelatin (FSG) for 45 min, followed by incubation with the primary antibody overnight at 4 °C. Collagen I (Abcam) antibody was diluted in a blocking buffer (0.2% FSG in PBS with 0.02% Tween20) at a dilution of 1:100. Finally, Alexa Flour 488/647 conjugated secondary antibodies corresponding specifically to the origin of the used primary antibody was added at 1:250 dilution and incubated for 45 min at 25 °C. The nuclei were counterstained with DAPI. The stained samples were observed under a confocal microscope (Zeiss Axio Observer Z1 LSM 700)

2.3.6 Scanning Electron Microscopy (SEM) and SEM-EDS (Energy Dispersive Spectroscopy)

3D fiber scaffolds seeded with MSCs and human osteoblast cells were incubated at 37°C, 5% CO_2 under humidified conditions for 21 days. The samples were washed with PBS, fixed using glutaraldehyde (2.5%), subsequently dehydrated using ethanol series (10% v/v, 30% v/v,50% v/v, 70% v/v, and 100%), and then dried with hexamethyldisilazane. SEM imaging was then performed on the dried samples after coating them with gold and mounting them on the SEM sample stubs. SEM-EDS experiments were also performed on these scaffolds.

2.4 Statistical Analysis

Two-way ANOVA, followed by Tukey's post hoc multiple comparison test, was used for statistical analysis. Data were considered significantly different when the probability values obtained were< 0.05 ($P < 0.05$). Quantitative data were expressed as a mean ± standard deviation. Triplicate samples were used for performing all the experiments.

3. RESULTS AND DISCUSSION

3.1 Microstructures of the polymer fibers

The PCL solutions were spun consecutively at 36 000 rpm at different pressures (no applied pressure, i.e., no gas flow and therefore gyration only, 0.1 MPa,0.2 MPa, 0.3 MPa) and also varying the concentration of MMT-Clay and HAP MMT-Clay (2 w/w % and 5 w/w %) to identify the effects of pressure and concentration on the microstructure of the fibers. The PCL fiber microstructures are characterized using scanning electron microscopy (SEM). (Fig. 1).

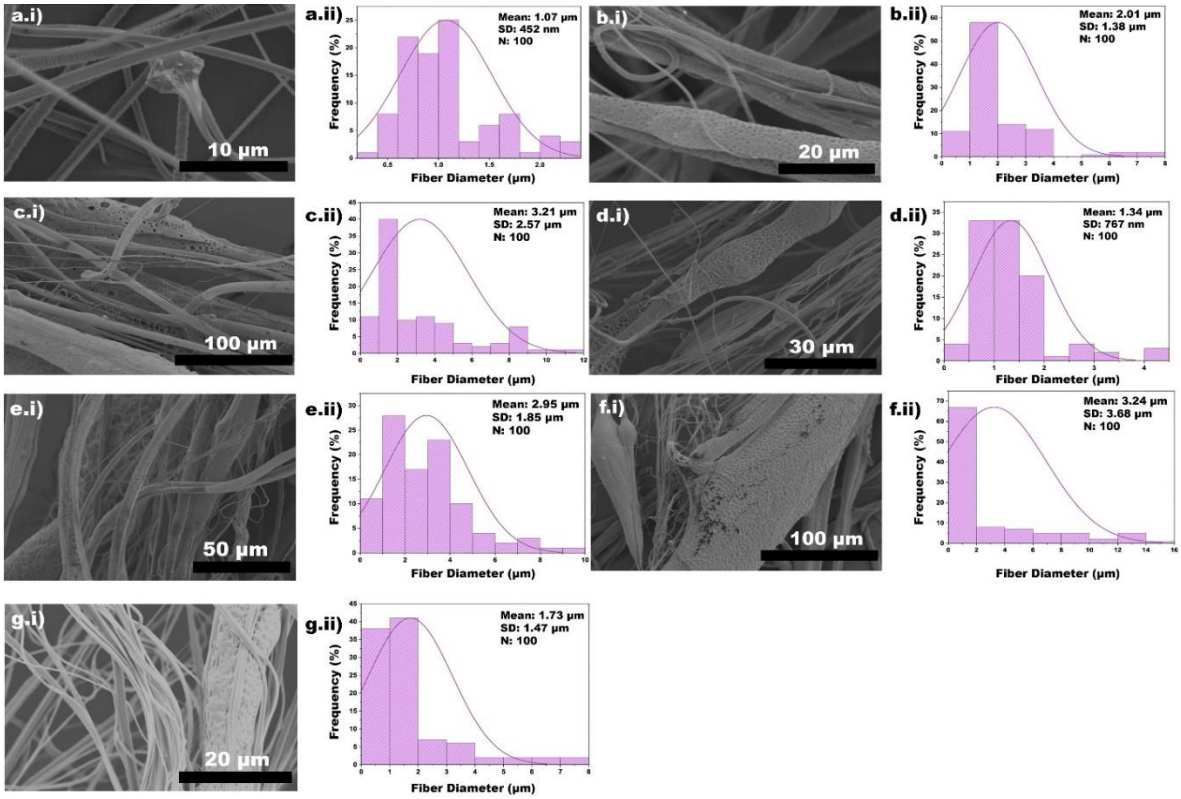

Fig. 1. SEM images of 15 w/v% PCL/ chloroform incorporated with: a.i) 2 w/w % MMT-Clay (0.3MPa), b.i) 5 w/w % MMT-Clay (0.3MPa), c.i) 5 w/w % MMT-Clay (no applied pressure), d.i) 2 w/w % HAP MMT-Clay (0.3MPa), e.i) 5 w/w % HAP MMT-Clay (0.3MPa), f.i) 5 w/w % HAP MMT-Clay (0 MPa), g.i) PCL/ chloroform (no applied pressure), and a.ii, b.ii, c.ii, d.ii, e.ii, f.ii, g.ii) respective fiber diameter distributions-all spun at 36,000 rpm.

The fiber size also increased with an increase in the nano-clay concentration. Interestingly, the formation of pores within fibers was observed to increase at higher HAP and MMT loading. The SEM images emphasized the alignment of PCL/ MMT and PCL/ HAP fibers. The morphology reveals the non-uniformity of fiber diameter across the fiber surface. PCL MMT-Clay fibers are observed as dark regions within the fiber strands, and PCL HAP MMT-Clay fibers are detected as blocks attached to the fiber pores. We also observe that the increase in the concentration of MMT-Clay (Fig. 1 a,b,c) results in an increase of the diameter of the fiber from 1.07 µm ± 452 nm to 3.21 µm ± 2.57 µm and increases the roughness of the fibers. It was also found that the increase in gas pressure significantly affects fiber diameter. In pressurize gyration, a gradient in the pressure results in accelerating the polymer solution out from the orifices. Therefore, an increase in gas pressure causes jet elongation resulting in fiber thinning; hence at higher gas pressures, usually thinner fibers are achieved. For the same concentration (5 w/w %) of the MMT-Clay (Fig. 1 b,c), with the reduction of pressure from 0.3 MPa to pressureless, the diameter of the fibers increases from 2.01 µm ± 1.38 µm to 3.21 µm ± 2.57. Similar effects of pressure and concentration were observed with HAP MMT-Clay. With the increase in the concentration from 2% to 5%; an increase in the diameter of the fibers from 1.34 µm ± 767 nm to 3.24 µm ± 3.68 µm (Fig. 1 d,e,f) is observed, resulting in the formation of thick HAP-Clay blocks embedded in the submicron fibrous structure and decrease in the pressure from 0.3 MPa to pressureless, at the same concentration (5%) increases the diameter of the fibers from 2.95 µm ± 1.85 µm to 3.24 µm ± 3.68 µm(Fig. 1 e,f).

3.2 Cell Viability

The WST-1 assay was performed to evaluate cell viability and proliferation of both MSCs and osteoblasts on the scaffolds to evaluate the biocompatibility of synthesized polymer fiber scaffolds over 21 days. The cell viability measured using the absorbance at 450 nm is proportional to the

amount of dehydrogenase activity in the cells[86]. Fig. 2 represents the cell viability of different fiber scaffolds seeded with MSCs and osteoblasts for 7 days, 14 days, and 21 days. We observed an increase in cell viability over time for all the three different scaffold systems. As compared to the control group (PCL fiber scaffolds), no significant increase in the cell viability was observed with PCL MMT-Clay fiber scaffolds at day 7 and day 14; however, at day 21 a significant increase was observed with PCL MMT-Clay fiber scaffolds.

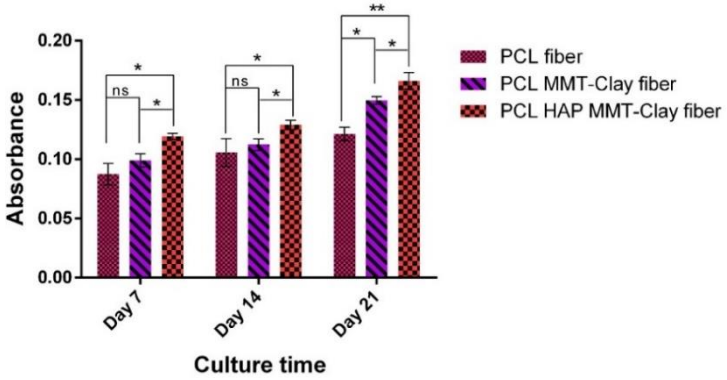

Fig. 2. Cell viability of scaffolds seeded with MSCs and osteoblast cells. (Two-way ANOVA followed by post hoc Tukey test $p^* < 0.05$, $p^{**} < 0.01$, $p^{***} < 0.001$, n = 3.)

Compared to the control group (PCL fiber scaffolds), a significant increase in the cell viability was observed with PCL HAP MMT-Clay fiber over 21 days. We also compared PCL HAP MMT-Clay fiber scaffolds with scaffolds PCL MMT-Clay fiber scaffolds and observed a significant increase in cell viability over 21 days. Collectively, the addition of HAP-Clay in the PCL fibers immensely enhanced the cell viability of the scaffolds.

3.3 Osteogenic Differentiation

Osteogenic differentiation of MSCs was assessed using the alkaline phosphatase (ALP) assay. Fig. 3a represents the ALP activity of fiber scaffolds seeded with MSCs and osteoblasts for 7 days, 14 days, and 21 days. Initially, we observed an increase in ALP activity over 14 days for all the three scaffold systems. This was followed by a gradual decline in ALP activity for all the samples. Compared to the control group (PCL fiber scaffolds), no significant increase in the ALP activity was observed with PCL MMT-Clay fiber scaffolds and PCL HAP MMT-Clay fiber scaffolds at day 7; however, at day 14 a

significant increase was observed with both PCL MMT-Clay fiber scaffolds and PCL HAP MMT-Clay fiber scaffolds. We also compared PCL HAP MMT-Clay fiber scaffolds with scaffolds PCL MMT-Clay fiber scaffolds; at day 7 no significant increase in ALP activity was observed; however, a significant increase with PCL HAP MMT-Clay fiber scaffolds was seen at day 14. A comparison of the ALP activity ALP activity on the PCL HAP MMT Clay fiber scaffolds seeded with only MSCs (5 X 10^4 MSCs were seeded on each scaffold) as compared to the co=culture with osteoblasts is shown in Fig. 3b. As seen, we observe a significant increase in ALP activity with MSCs till day 14, followed by a decrease in the ALP activity. On day 7, the ALP activity in the osteoblast-MSC co-culture has contributions from both MSCs and osteoblasts. However, on day 14 and day 21, a significant portion of the ALP activity arises from the osteogenic differentiation of MSCs.

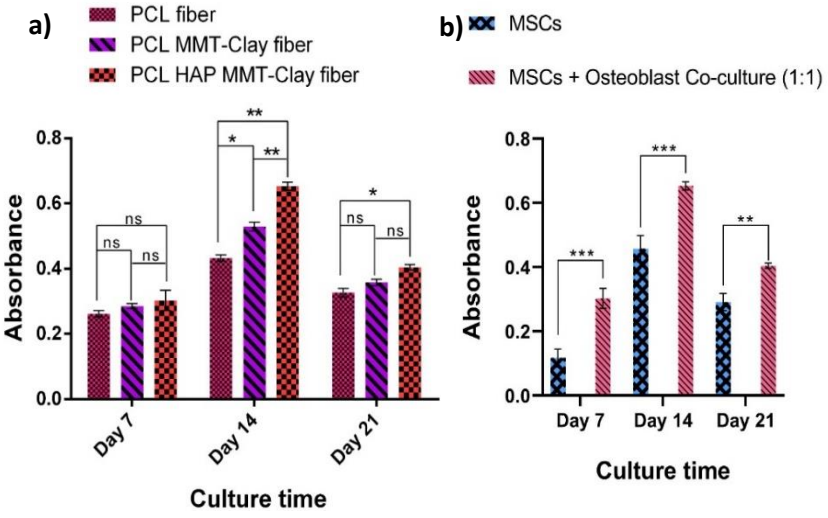

Fig. 3. ALP activity of scaffolds seeded with (a) MSCs and osteoblast cells and (b) Only MSCs and co-culture of MSCs and Osteoblast (1:1). *Two-way ANOVA followed by post hoc Tukey test p*<0.05, p**<0.01, p***<0.001, n=3)*

The initial increase in the ALP activity till 14 days indicates that, initially, the rate of differentiation of MSCs into osteoblast phenotype was higher. The decrease in ALP activity indicates the fewer number of MSCs differentiated into osteoblast phenotype. It has been reported that the ALP activity of MSCs decreases during osteogenic differentiation[87]. A similar ALP activity of MSCs is reported in literature over the same time period [88]. Results indicate that HAP-Clay in the PCL fibers very significantly enhanced the ALP activity of the scaffolds.

3.4 Bone mineralization

The Alizarin red S (ARS) staining was performed to check the formation of the mineralized extracellular matrix (ECM) on the polymeric fiber scaffolds (Fig. 4). The red color formation with Alizarin red S indicates the deposition of the inorganic matrix by cells cultured on scaffolds. Prior studies have shown calcium deposition increases over time in PCL/ in situ HAP clay scaffold seeded with MSCs over 23 days[89]. As seen in Fig. 4, ARS staining showed dispersed and limited calcium deposition at 7 days, while enhanced calcium deposition was observed at 21 days (Fig. 4a), which was further confirmed by quantification of the released ARS (Fig. 4b).

Over time, calcium deposition increases in all the fiber scaffold systems. Compared to the control group (PCL fiber scaffolds), no significant increase in the calcium deposition was observed with PCL MMT-Clay fiber scaffolds and PCL HAP MMT-Clay fiber scaffolds at day 7.

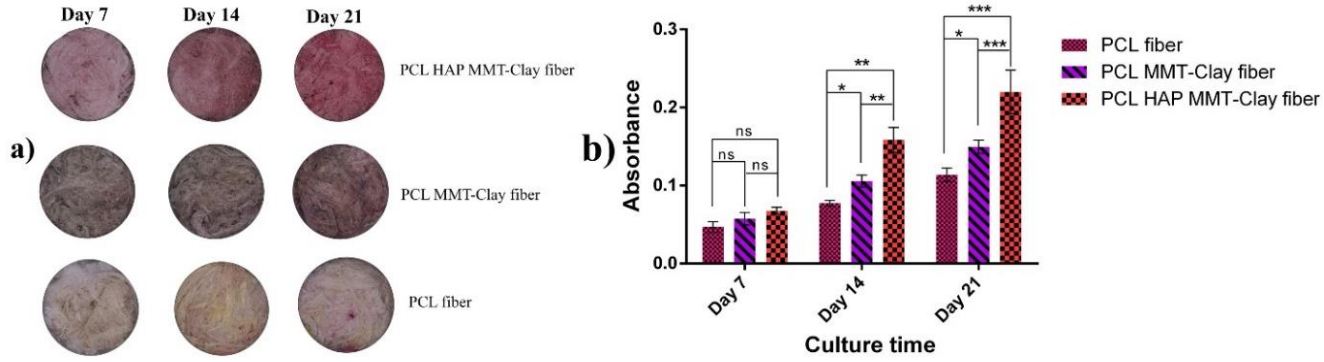

Fig. 4. Alizarin Red S staining (a) and quantification absorbance assay (b) of scaffolds seeded with MSCs and osteoblast cells.

However, at day 14 and day 21, a significant increase with both PCL MMT-Clay fiber scaffolds and PCL HAP MMT-Clay fiber scaffolds was observed. A significant increase in the mineral deposition was observed with PCL HAP MMT-Clay fiber scaffolds compared to PCL MMT-Clay fiber scaffolds. Hence, the addition of HAP-Clay in the PCL fibers enhanced the mineral deposition of the scaffolds.

3.5 Collagen and collagen fibril formation

Immunocytochemistry assay was performed to evaluate the formation of collagen. The appearance of green color indicates the formation of the collagen by primary- secondary antigen-antibody interaction. A prior study [18] reported that collagen's well-defined fibril structure is observed at 11 days for PCL/in situ HAP clay scaffolds seeded with MSCs and osteoblast cells coated with bone morphogenic proteins. Fig. 5. shows confocal microscope images of PCL fibers scaffold, PCL MMT-Clay fibers scaffold, PCL HAPMMT-Clay fibers scaffold seeded with MSCs and osteoblasts at day 21.

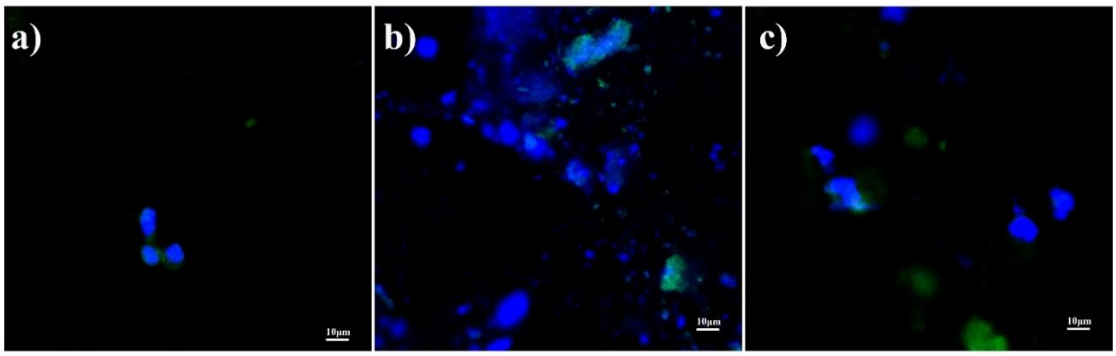

Fig. 5. Confocal microscope image of a) PCL fiber, b) PCL MMT-Clay fiber, c) PCL HAP MMT-Clay fiber scaffolds seeded with MSCs & osteoblasts at day 21. Nuclei were stained with DAPI (blue). Anti-rabbit Col-1 primary antibody was used with goat anti-rabbit IgG (H + L) AF 488 (green) secondary antibody.

We observe the least collagen formation in scaffolds with PCL fibers and the highest with PCL HAP MMT-Clay fibers. Thus it appears that HAP-Clay particles actively induce collagen formation.

3.6 Scanning Electron Microscopy (SEM) studies

To investigate the morphology of cells at the different fiber scaffolds, SEM imaging was performed. Fig. 6 shows the SEM images of a) PCL fibers, b) PCL MMT-Clay fibers, c) PCL HAP MMT-Clay fiber scaffolds seeded with MSCs and osteoblasts at day 21. As seen, a flattened morphology of the cells was observed in the surface of the fibers indicated with red circles/ellipses; More cells were observed with PCL HAP MMT-Clay fiber scaffolds.

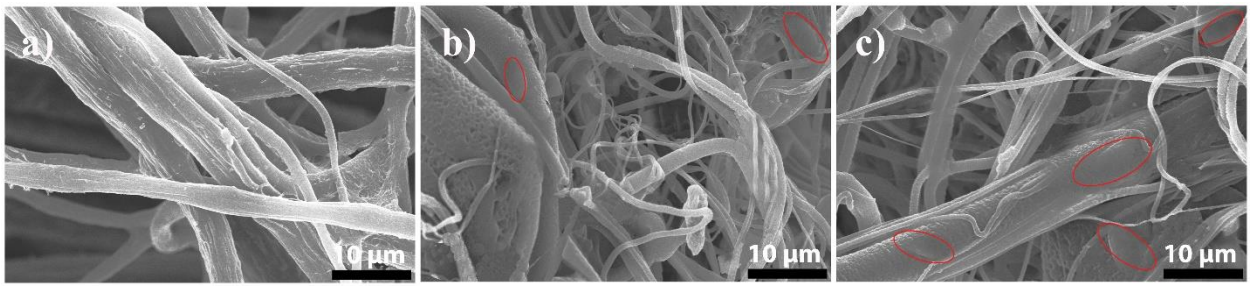

Fig. 6. SEM micrographs of a) PCL fiber, b) PCL MMT-Clay fiber, c) PCL HAP MMT-Clay fiber scaffolds seeded with MSCs and osteoblasts at day 21 (red circles/ellipses represent flattened cells on the surface of the fibers).

3.7 Elemental composition of nanocomposite fibers

As determined by EDS, fiber samples indicate elemental constituents of carbon, sodium, silicon, chloride, gold, and calcium. The source of the sodium and chloride in the spectrum is the entrapped NaCl in the fibers from the cell culture medium, and the source of the gold is the coating. The elemental spectrum of the PCL MMT-Clay fibers is shown in Fig. 7a. The presence of Si in this spectrum indicates the dispersion of the clay particles (montmorillonite) in the fibers. The elemental spectrum of the PCL HAP MMT-Clay fibers is shown in Fig.7b. The presence of Si and Ca in this spectrum indicates the dispersion of the HAP-clay particles in the fibers. The results indicate the formation of composites of PCL with HAP MMT-Clay through the pressurized gyration method.

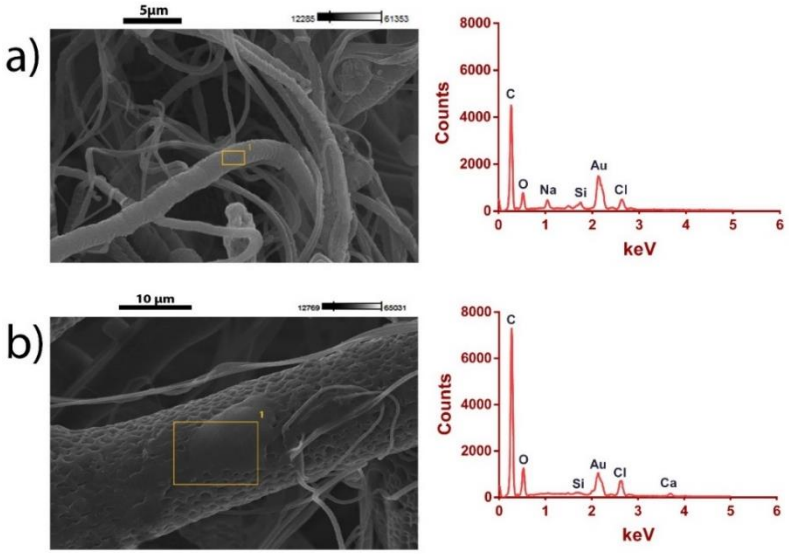

Fig. 7. Elemental spectra of a) PCL MMT-Clay fiber, b) PCL HAP MMT-Clay fiber, yellow boxes shown in left-hand side images represent the spots from

which localized elemental data were obtained during SEM-EDS experiments.

4. CONCLUSIONS

This comprehensive investigation demonstrates novel methods for the fabrication of HAP nanoclay PCL composite fibers for bone tissue regeneration applications. Using a pressurized gyration setup, we fabricated PCL fibers incorporated with nano HAP MMT-Clay and nano MMT-Clay at 2 w/w% and 5 w/w%. The results demonstrated that the polymer fiber scaffolds as prepared are biocompatible; cells were able to thrive and differentiate on the fiber scaffolds.

Calcium deposition and collagen formation, the main components of ECM formation, were also observed. The addition of HAP-Clay was found to enhance the cell viability and proliferation of cells on PCL fiber scaffolds. Further, the intracellular ALP levels increased with PCL HAP MMT-Clay fiber scaffold, indicating enhancement of the osteogenic differentiation of MSCs. Immunocytochemistry was also performed to evaluate the formation of the collagen in the PCL fiber scaffolds. PCL HAP MMT-Clay fibers scaffold showed enhanced collagen formation as opposed to control, PCL fiber scaffolds. Compressed pellets of the nanoclay HAP polymer fibers fabricated here have potential applications as fillers for non-union bone defects and their use as 'cement' for non-union scaffold preparations for bone tissue regeneration.

Acknowledgments

The Katti and Katti lab would like to acknowledge support from NSF (OIA NDACES-1946202) and the ND Department of Commerce (Grant 19-11-G-237). Edirisinghe-lab wishes to thank the UK Engineering and Physical Sciences Research Council for funding pressurized gyration research at UCL (Grants: EP/S016872/1, EP/N034228/1, and EP/L023059/1).

REFERENCES

[1] Z. Sheikh, N. Hamdan, Y. Ikeda, M. Grynpas, B. Ganss, M. Glogauer, Natural graft tissues and synthetic biomaterials for periodontal and alveolar bone reconstructive applications: a review, Biomater. Res.

21(9) (2017) 1-20.

[2] G. Fernandez de Grado, L. Keller, Y. Idoux-Gillet, Q. Wagner, A.M. Musset, N. Benkirane-Jessel, F. Bornert, D. Offner, Bone substitutes: a review of their characteristics, clinical use, and perspectives for large bone defects management, J. Tissue Eng. 9 (2018) 1-18.

[3] S. Titsinides, G. Agrogiannis, T. Karatzas, Bone grafting materials in dentoalveolar reconstruction: A comprehensive review, Jpn. Dent. Sci. Rev. 55 (2019) 26–32.

[4] H.-S. Sohn, J.-K. Oh, Review of bone graft and bone substitutes with an emphasis on fracture surgeries, Biomater. Res. 23(9) (2019) 1-7.

[5] I. Bružauskaitė, D. Bironaitė, E. Bagdonas, E. Bernotienė, Scaffolds and cells for tissue regeneration: different scaffold pore sizes—different cell effects, Cytotechnology. 68 (2016) 355–369.

[6] M. Rasoulianboroujeni, N. Kiaie, F.S. Tabatabaei, A. Yadegari, F. Fahimipour, K. Khoshroo, L. Tayebi, Dual Porosity Protein-based Scaffolds with Enhanced Cell Infiltration and Proliferation, Sci. Rep. 8 (2018) 14889.

[7] M. Ansari, Bone tissue regeneration: biology, strategies and interface studies, Prog. Biomater. 8 (2019) 223–237.

[8] Y. Wang, W. Cui, X. Zhao, S. Wen, Y. Sun, J. Han, H. Zhang, Bone remodeling-inspired dual delivery electrospun nanofibers for promoting bone regeneration, Nanoscale. 11 (2019) 60–71.

[9] Y.F. Goh, I. Shakir, R. Hussain, Electrospun fibers for tissue engineering, drug delivery, and wound dressing, J. Mater. Sci. 48 (2013) 3027–3054.

[10] A. Ali, S. Bano, S.S. Poojary, D. Kumar, Y.S. Negi, Effect of incorporation of montmorillonite on Xylan/Chitosan conjugate scaffold, Colloids Surfaces B Biointerfaces. 180 (2019) 75–82.

[11] S.E. Enderami, S.F. Ahmadi, R.N. Mansour, S. Abediankenari, H. Ranjbaran, M. Mossahebi-Mohammadi, R. Salarinia, H. Mahboudi, Electrospun silk nanofibers improve differentiation potential of human induced pluripotent stem cells to insulin producing cells, Mater. Sci. Eng. C. 108 (2020) 110398.

[12] T. Ghassemi, A. Shahroodi, M.H. Ebrahimzadeh, A. Mousavian, J. Movaffagh, A. Moradi, Current concepts in scaffolding for bone tissue engineering, Arch. Bone Jt. Surg. 6 (2018) 90–99.

[13] S. Stratton, N.B. Shelke, K. Hoshino, S. Rudraiah, S.G. Kumbar, Bioactive polymeric scaffolds for tissue engineering, Bioact. Mater. 1 (2016) 93–108.

[14] J.-H. Zeng, S.-W. Liu, L. Xiong, P. Qiu, L.-H. Ding, S.-L. Xiong, J.-T. Li, X.-G. Liao, Z.-M. Tang, Scaffolds for the repair of bone defects in clinical studies: a systematic review, J. Orthop. Surg. Res. 13(33) (2018) 1-14.

[15] A. Sharikova, Z.I. Foraida, L. Sfakis, L. Peerzada, M. Larsen, J. Castracane, A. Khmaladze, Characterization of nanofibers for tissue engineering: Chemical mapping by Confocal Raman microscopy, Spectrochim. Acta Part A Mol. Biomol. Spectrosc. 227 (2020) 117670.

[16] Haryanto, S. Kim, J.H. Kim, J.O. Kim, S. Ku, H. Cho, D.H. Han, P. Huh, Fabrication of poly(ethylene oxide) hydrogels for wound dressing application using E-beam, Macromol. Res. 22 (2014) 131–138.

[17] A. Nauth, M.D. McKee, T.A. Einhorn, J.T. Watson, R. Li, E.H. Schemitsch, Managing bone defects, J. Orthop. Trauma. 25 (2011) 462–466.

[18] K. Kundu, D.R. Katti, K.S. Katti, Tissue-Engineered Interlocking Scaffold Blocks for the Regeneration of Bone, JOM. 72 (2020) 1443–1457.

[19] M. Van Lieshout, G. Peters, M. Rutten, F. Baaijens, A knitted, fibrin-covered polycaprolactone scaffold for tissue engineering of the aortic valve, Tissue Eng. 12 (2006) 481–487.

[20] D. Li, T. Wu, N. He, J. Wang, W. Chen, L. He, C. Huang, H.A. EI-Hamshary, S.S. Al-Deyab, Q. Ke, X. Mo, Three-dimensional polycaprolactone scaffold via needleless electrospinning promotes cell proliferation and infiltration, Colloids Surfaces B Biointerfaces. 121 (2014) 432–443.

[21] J. Zhao, W. Han, H. Chen, M. Tu, R. Zeng, Y. Shi, Z. Cha, C. Zhou, Preparation, structure and crystallinity of chitosan nano-fibers by a solid–liquid phase separation technique, Carbohydr. Polym. 83 (2011) 1541–1546.

[22] S.L. Tao, T.A. Desai, Aligned Arrays of Biodegradable Poly(ε-caprolactone) Nanowires and Nanofibers by Template Synthesis, Nano Lett. 7 (2007) 1463–1468.

[23] L.E.R. O'Leary, J.A. Fallas, E.L. Bakota, M.K. Kang, J.D. Hartgerink, Multi-hierarchical self-assembly of a collagen mimetic peptide from triple helix to nanofibre and hydrogel, Nat. Chem. 3 (2011) 821–828.

[24] P. Sofokleous, E. Stride, M. Edirisinghe, Preparation, Characterization, and Release of Amoxicillin from Electrospun Fibrous Wound Dressing Patches, Pharm. Res. 30 (2013) 1926–1938.

[25] U.E. Illangakoon, H. Gill, G.C. Shearman, M. Parhizkar, S. Mahalingam, N.P. Chatterton, G.R. Williams, Fast dissolving paracetamol/caffeine nanofibers prepared by electrospinning, Int. J. Pharm. 477 (2014) 369–379.

[26] G. Narayanan, B.S. Gupta, A.E. Tonelli, Poly(ε-caprolactone) nanowebs functionalized with α- And γ-cyclodextrins, Biomacromolecules. 15 (2014) 4122–4133.

[27] J. Ren, K.A. Blackwood, A. Doustgani, P.P. Poh, R. Steck, M.M. Stevens, M.A. Woodruff, Melt-electrospun polycaprolactone strontium-substituted bioactive glass scaffolds for bone regeneration, J. Biomed. Mater. Res. Part A. 102 (2014) 3140–3153.

[28] D. Sankar, K.T. Shalumon, K.P. Chennazhi, D. Menon, R. Jayakumar, Surface plasma treatment of poly(caprolactone) micro, nano, and multiscale fibrous scaffolds for enhanced osteoconductivity, Tissue Eng. - Part A. 20 (2014) 1689–1702.

[29] W. Liu, S. Thomopoulos, Y. Xia, Electrospun Nanofibers for Regenerative Medicine, Soft Fibrillar Materials: Fabrication and Applications, Chapter 9 (2013) 265–295.

[30] V. Beachley, E. Katsanevakis, N. Zhang, X. Wen, A Novel Method to Precisely Assemble Loose Nanofiber Structures for Regenerative Medicine Applications, Adv. Healthc. Mater. 2 (2013) 343–351.

[31] C.J. Luo, S.D. Stoyanov, E. Stride, E. Pelan, M. Edirisinghe, Electrospinning versus fibre production methods: From specifics to technological convergence, Chem. Soc. Rev. 41 (2012) 4708–4735.

[32] H. Alenezi, M.E. Cam, M. Edirisinghe, Experimental and theoretical investigation of the fluid behavior during polymeric fiber formation with and without pressure, Appl. Phys. Rev. 6 (2019) 041401.

[33] S. Mahalingam, G.G. Ren, M.J. Edirisinghe, Rheology and pressurised gyration of starch and starch-loaded poly(ethylene oxide), Carbohydr. Polym. 114 (2014) 279–287.

[34] B.T. Raimi-Abraham, S. Mahalingam, P.J. Davies, M. Edirisinghe, D.Q.M. Craig, Development and Characterization of Amorphous Nanofiber Drug Dispersions Prepared Using Pressurized Gyration, Mol. Pharm. 12 (2015) 3851–3861.

[35] B.T. Raimi-Abraham, S. Mahalingam, M. Edirisinghe, D.Q.M. Craig, Generation of poly(N-vinylpyrrolidone) nanofibres using pressurised gyration, Mater. Sci. Eng. C. 39 (2014) 168–176.

[36] P. Prabhu, Nanofibers for Medical Diagnosis and Therapy, in: A. Barhoum, M. Bechelany, A.S.H. Makhlouf (Eds.), Handb. Nanofibers, Springer International Publishing, Cham. (2019) 831–867.

[37] A. Memic, T. Abudula, H.S. Mohammed, K. Joshi Navare, T. Colombani, S.A. Bencherif, Latest Progress in Electrospun Nanofibers for Wound Healing Applications, ACS Appl. Bio Mater. 2 (2019) 952–969.

[38] S.P. Miguel, R.S. Sequeira, A.F. Moreira, C.S.D. Cabral, A.G. Mendonça, P. Ferreira, I.J. Correia, An overview of electrospun membranes loaded with bioactive molecules for improving the wound healing process, Eur. J. Pharm. Biopharm. 139 (2019) 1–22.

[39] A. Barhoum, K. Pal, H. Rahier, H. Uludag, I.S. Kim, M. Bechelany, Nanofibers as new-generation materials: From spinning and nano-spinning fabrication techniques to emerging applications, Appl. Mater. Today. 17 (2019) 1–35.

[40] S. Ahn, H.A.M. Ardoña, P.H. Campbell, G.M. Gonzalez, K.K. Parker, Alfalfa Nanofibers for Dermal Wound Healing, ACS Appl. Mater. Interfaces. 11 (2019) 33535–33547.

[41] I.S. Kurtz, J.D. Schiffman, Current and emerging approaches to engineer antibacterial and antifouling electrospun nanofibers, Materials (Basel). 11 (2018) 1059.

[42] S. Nemati, S. jeong Kim, Y.M. Shin, H. Shin, Current progress in application of polymeric nanofibers to tissue engineering, Nano Converg. 6 (2019) 1–16.

[43] F. Paladini, M. Pollini, Antimicrobial silver nanoparticles for wound healing application: Progress and future trends, Materials (Basel). 12 (2019) 2540.

[44] S. Ahn, C.O. Chantre, A.R. Gannon, J.U. Lind, P.H. Campbell, T. Grevesse, B.B. O'Connor, K.K. Parker, Soy Protein/Cellulose Nanofiber Scaffolds Mimicking Skin Extracellular Matrix for Enhanced Wound Healing, Adv. Healthc. Mater. 7 (2018) 1701175.

[45] J. Ko, N.K. Mohtaram, F. Ahmed, A. Montgomery, M. Carlson, P.C.D. Lee, S.M. Willerth, M.B.G. Jun, Fabrication of poly (ε-caprolactone) microfiber scaffolds with varying topography and mechanical properties for stem cell-based tissue engineering applications, J. Biomater. Sci. Polym. Ed. 25 (2014) 1–17.

[46] M.J. Mochane, T.S. Motsoeneng, E.R. Sadiku, T.C. Mokhena, J.S. Sefadi, Morphology and properties of electrospun PCL and its composites for medical applications: A mini review, Appl. Sci. 9 (2019) 2205.

[47] S.Y. Reyes-López, D. Cornejo-Monroy, G. González-García, A Novel Route for the Preparation of Gold Nanoparticles in Polycaprolactone Nanofibers, J. Nanomater. 2015 (2015) 1–7.

[48] D. Chuan, R. Fan, Y. Wang, Y. Ren, C. Wang, Y. Du, L. Zhou, J. Yu, Y. Gu, H. Chen, G. Guo, Stereocomplex poly(lactic acid)-based composite nanofiber membranes with highly dispersed hydroxyapatite for potential bone tissue engineering, Compos. Sci. Technol. 192 (2020) 108107.

[49] Y.S. Cho, M. Quan, S.H. Lee, M.W. Hong, Y.Y. Kim, Y.S. Cho, Assessment of osteogenesis for 3D-printed polycaprolactone/hydroxyapatite composite scaffold with enhanced exposure of hydroxyapatite using rat calvarial defect model, Compos. Sci. Technol. 184 (2019) 107844.

[50] P. Melo, A.M. Ferreira, K. Waldron, T. Swift, P. Gentile, M. Magallanes, M. Marshall, K. Dalgarno, Osteoinduction of 3D printed particulate and short-fibre reinforced composites produced using PLLA and apatite-wollastonite, Compos. Sci. Technol. 184 (2019) 107834.

[51] R. Langer, J.P. Vacanti, Tissue engineering, Science. 260 (1993) 920–926.

[52] S. Bose, S. Dasgupta, S. Tarafder, A. Bandyopadhyay, Microwave-processed nanocrystalline hydroxyapatite: Simultaneous enhancement of mechanical and biological properties, Acta Biomater. 6 (2010) 3782–3790.

[53] G.E. Poinern, R.K. Brundavanam, N. Mondinos, Z.T. Jiang, Synthesis and characterisation of nanohydroxyapatite using an ultrasound assisted method, Ultrason. Sonochem. 16 (2009) 469–474.

[54] R.Z. LeGeros, Calcium phosphate-based osteoinductive materials, Chem. Rev. 108 (2008) 4742–4753.

[55] M.P. Ginebra, M. Espanol, E.B. Montufar, R.A. Perez, G. Mestres, New processing approaches in calcium phosphate cements and their applications in regenerative medicine, Acta Biomater. 6 (2010) 2863–2873.

[56] R. Nawang, M.Z. Hussein, K.A. Matori, C.A. Che Abdullah, M. Hashim, Physicochemical properties of hydroxyapatite/montmorillonite nanocomposite prepared by powder sintering, Results Phys. 15 (2019) 102540.

[57] A.H. Ambre, D.R. Katti, K.S. Katti, Biomineralized hydroxyapatite nanoclay composite scaffolds with polycaprolactone for stem cell-based bone tissue engineering, J. Biomed. Mater. Res. - Part A. 103 (2015) 2077–2101.

[58] G. Wu, F. Huang, Y. Huang, Y. Chen, L. Zheng, H. Wang, Y. Xie, Bone inductivity comparison of control versus non-control released rhBMP2 coatings in 3D printed hydroxyapatite scaffold, J. Biomater. Appl. 34 (2020) 1254–1266.

[59] B. Huang, C. Vyas, J.J. Byun, M. El-Newehy, Z. Huang, P. Bártolo, Aligned multi-walled carbon nanotubes with nanohydroxyapatite in a 3D printed polycaprolactone scaffold stimulates osteogenic differentiation, Mater. Sci. Eng. C. 108 (2020) 110374.

[60] S. Bose, G. Fielding, S. Tarafder, A. Bandyopadhyay, Understanding of dopant-induced osteogenesis and angiogenesis in calcium phosphate ceramics, Trends Biotechnol. 31 (2013) 594–605.

[61] S. Bose, G. Fielding, S. Tarafder, A. Bandyopadhyay, Trace element doping in calcium phosphate ceramics to understand osteogenesis and angiogenesis, Trends Biotechnol. 18 (2013) 1199–1216.

[62] C. Dai, H. Guo, J. Lu, J. Shi, J. Wei, C. Liu, Osteogenic evaluation of calcium/magnesium-doped mesoporous silica scaffold with incorporation of rhBMP-2 by synchrotron radiation-based μCT, Biomaterials. 32 (2011) 8506–8517.

[63] S. Bose, S. Tarafder, A. Bandyopadhyay, Effect of Chemistry on Osteogenesis and Angiogenesis Towards Bone Tissue Engineering Using 3D Printed Scaffolds, Ann. Biomed. Eng. 45 (2017) 261–272.

[64] V. Mittal, Polymer layered silicate nanocomposites: A review, Materials (Basel). 2 (2009) 992–1057.

[65] S. Sinha Ray, M. Okamoto, Polymer/layered silicate nanocomposites: A review from preparation to processing, Prog. Polym. Sci. 28 (2003) 1539–1641.

[66] K.S. Katti, D.R. Katti, R. Dash, Synthesis and characterization of a novel chitosan/montmorillonite/ hydroxyapatite nanocomposite for bone tissue engineering, Biomed. Mater. 3 (2008) 034122.

[67] A.J. Mieszawska, J.G. Llamas, C.A. Vaiana, M.P. Kadakia, R.R. Naik, D.L. Kaplan, Clay enriched silk biomaterials for bone formation, Acta Biomater. 7 (2011) 3036–3041.

[68] A.H. Ambre, D.R. Katti, K.S. Katti, Nanoclays mediate stem cell differentiation and mineralized ECM

formation on biopolymer scaffolds, J. Biomed. Mater. Res. Part A. 101A (2013) 2644–2660.

[69] Y. Shi, G. Hu, J. Su, W. Li, Q. Chen, P. Shou, C. Xu, X. Chen, Y. Huang, Z. Zhu, X. Huang, X. Han, N. Xie, G. Ren, Mesenchymal stem cells: a new strategy for immunosuppression and tissue repair, Cell Res. 20 (2010) 510–518.

[70] D.J. Prockop, Marrow stromal cells as stem cells for nonhematopoietic tissues, Science. 276 (1997) 71–74.

[71] S.E. Haynesworth, J. Goshima, V.M. Goldberg, A.I. Caplan, Characterization of cells with osteogenic potential from human marrow, Bone. 13 (1992) 81–88.

[72] G.H. Altman, R.L. Horan, I. Martin, J. Farhadi, P.R.H. Stark, V. Volloch, J.C. Richmond, G. Vunjak-Novakovic, D.L. Kaplan, Cell differentiation by mechanical stress, FASEB J. 16 (2002) 1–13.

[73] J.N. Beresford, J.H. Bennett, C. Devlin, M.E. Owen, Evidence for an inverse relationship between the differentiation of adipocytic and osteogenic cells, Bone Miner. 17 (1992) 198.

[74] S. Wakitani, T. Goto, S.J. Pineda, R.G. Young, J.M. Mansour, A.I. Caplan, V.M. Goldberg, Mesenchymal cell-based repair of large, full-thickness defects of articular cartilage., J. Bone Jt. Surg. 76 (1994) 579–592.

[75] B. Johnstone, T.M. Hering, A.I. Caplan, V.M. Goldberg, J.U. Yoo, In vitro chondrogenesis of bone marrow-derived mesenchymal progenitor cells, Exp. Cell Res. 238 (1998) 265–272.

[76] S. Wakitani, T. Saito, A.I. Caplan, Myogenic cells derived from rat bone marrow mesenchymal stem cells exposed to 5-azacytidine, Muscle Nerve. 18 (1995) 1417–1426.

[77] H. Petite, V. Viateau, W. Bensaïd, A. Meunier, C. de Pollak, M. Bourguignon, K. Oudina, L. Sedel, G. Guillemin, Tissue-engineered bone regeneration, Nat. Biotechnol. 18 (2000) 959–963.

[78] E. Kon, A. Muraglia, A. Corsi, P. Bianco, M. Marcacci, I. Martin, A. Boyde, I. Ruspantini, P. Chistolini, M. Rocca, R. Giardino, R. Cancedda, R. Quarto, Autologous bone marrow stromal cells loaded onto porous hydroxyapatite ceramic accelerate bone repair in critical-size defects of sheep long bones, J. Biomed. Mater. Res. 49 (2000) 328–337.

[79] L.C. Gerstenfeld, J. Cruceta, C.M. Shea, K. Sampath, G.L. Barnes, T.A. Einhorn, Chondrocytes Provide Morphogenic Signals That Selectively Induce Osteogenic Differentiation of Mesenchymal Stem Cells, J. Bone Miner. Res. 17 (2002) 221–230.

[80] J.M. Dayer, P. Isler, L.P. Nicod, Adhesion molecules and cytokine production, Am. Rev. Respir. Dis. 148 (1993) S70–S74.

[81] R. Civitelli, Cell-Cell Communication in Bone, Calcif. Tissue Int. 56 (1995) S29–S31.

[82] K.S. Katti, A.H. Ambre, N. Peterka, D.R. Katti, Use of unnatural amino acids for design of novel organomodified clays as components of nanocomposite biomaterials, Philos. Trans. R. Soc. A Math. Phys. Eng. Sci. 368 (2010) 1963–1980

[83] A.H. Ambre, K.S. Katti, D.R. Katti, Nanoclay Based Composite Scaffolds for Bone Tissue Engineering Applications, J. Nanotechnol. Eng. Med. 1 (2010) 031013.

[84] K.S. Katti, D.R. Katti, A.H. Ambre, Unnatural amino acids modified clays for design of scaffolds for bone tissue engineering, in: Proc. ASME 1st Glob. Congr. Nanoeng. Med. Biol. NEMB2010, American Society of Mechanical Engineers Digital Collection. (2010) 227–228.

[85] A. Ambre, K.S. Katti, D.R. Katti, In situ mineralized hydroxyapatite on amino acid modified nanoclays as novel bone biomaterials, Mater. Sci. Eng. C. 31 (2011) 1017–1029.

[86] A.H. Cory, T.C. Owen, J.A. Barltrop, J.G. Cory, Use of an aqueous soluble tetrazolium/formazan assay for cell growth assays in culture, Cancer Commun. 3 (1991) 207–212.

[87] Richard A. Thibault, L. Scott Baggett, Antonios G. Mikos, F. Kurtis Kasper, Osteogenic Differentiation of Mesenchymal Stem Cells on Pregenerated Extracellular Matrix Scaffolds in the Absence of Osteogenic Cell Culture Supplements, Tissue Eng. Part A, 16 (2010) 431–440.

[88] Eeva Castrén, Tarvo Sillat, Sofia Oja, Ariel Noro, Anita Laitinen, Yrjö T Konttinen, Petri Lehenkari, Mika Hukkanen & Matti Korhonen, Osteogenic differentiation of mesenchymal stromal cells in two-dimensional and three-dimensional cultures without animal serum, Stem Cell Research & Therapy, 6(2015) 167.

[89] S. Kar, H. Jasuja, D.R. Katti, K.S. Katti, Wnt/β-Catenin Signaling Pathway Regulates Osteogenesis for Breast Cancer Bone Metastasis: Experiments in an In Vitro Nanoclay Scaffold Cancer Testbed, ACS Biomater. Sci. Eng. 6 (2020) 2600–2611.